

Effect of the crust on neutron star empirical relations

Márcio Ferreira^{1,*} and Constança Providência^{1,†}

¹*CFisUC, Department of Physics, University of Coimbra, P-3004 - 516 Coimbra, Portugal*

(Dated: October 13, 2020)

We analyze how the crust equation of state affects several neutron star properties and how it impacts on possible constraints inferred from astrophysical observations. Using three distinct crusts, we generate three sets of model-independent equations of state describing stellar matter from a Taylor expansion around saturation density. The equations of state are thermodynamically consistent, causal, and compatible with astrophysical observations. The relations between the tidal deformability Λ and compactness C , Love number k_2 and radius of neutron star with mass M are studied, and the effect of the crust equation of state on these relations analyzed. In most of the relations, the impact of the crust equation of state is not larger than 2%. If, however, a fixed neutron star mass is considered, the relation between the tidal deformability and the radius depends on the crust. We have found that the relation $\Lambda_{M_i} = \alpha R_{M_i}^\beta$ becomes almost exact and crust independent for massive neutron stars. It is shown that it is possible to determine the tidal deformability of an $1.4M_\odot$ star from the GW179817 effective tidal deformability $\tilde{\Lambda}$ with an accuracy of at least $\approx 10\%$. A high correlation between $\tilde{\Lambda}$ and the radius of the most massive star of the neutron star binary was confirmed, however, it was demonstrated that the crust has an effect of $\approx 14\%$ on this relation. We have found that the relation $\Lambda_1/\Lambda_2 = q^a$ depends on M_{chirp} as $a \sim \sqrt{M_{\text{chirp}}}$.

I. INTRODUCTION

Our knowledge on the equation of state (EoS) of nuclear matter is still very limited. Its properties above the nuclear saturation density remain an open question in nuclear physics. Neutron stars (NSs) are special astrophysical objects through which the properties of cold super-dense neutron-rich nuclear matter can be investigated. Some massive NSs observed during the last decade established quite stiff constraints on the EoS of nuclear matter. The pulsar PSR J1614–2230 is the one with the smallest uncertainty on the mass $M = 1.908 \pm 0.016 M_\odot$ [1–3]. Two known pulsars with a mass above two solar masses are PSR J0348+0432 with $M = 2.01 \pm 0.04 M_\odot$ [4] and the recently detected MSP J0740+6620 with a mass $2.14^{+0.10}_{-0.09} M_\odot$ [5]. The simultaneous measurement of the mass and radius of a NS with an uncertainty of the order of 5% is one of the objectives of the already operating NICER mission [6] and of some of the planned x-ray observatories like the Athena x-ray telescope [7] and the eXTP mission [8]. Recently, the mass and radius of the pulsar PSR J0030-0451 has been determined by two different teams of NICER [9, 10], however, still with a larger uncertainty. It is also expected that the number of known pulsars, and possibly also pulsars in binary systems, will increase enormously when the radio-telescope SKA [11] will be fully operating.

The gravitational waves (GWs) emitted during the coalescence of binary NS systems carry important information on the high density properties of the EoS. The analysis of the compact binary inspiral event GW170817 has settled an upper bound on the effective tidal deformabil-

ity of the binary $\tilde{\Lambda}$ [12]. Using a low-spin prior, which is consistent with the observed NS population, the value $\tilde{\Lambda} \leq 800$ (with 90% confidence) was determined from the GW170817 event. Tighter constraints were found in a follow up reanalysis [13], with $\tilde{\Lambda} = 300^{+420}_{-230}$ (using the 90% highest posterior density interval), under minimal assumptions about the nature of the compact objects. The two NS radii for the GW170817 event were estimated in [14], under the hypothesis that both NS are described by the same EoS and have spins within the range observed in Galactic binary NSs, to be $R_1 = 11.9^{+1.4}_{-1.4}$ km (heavier star) and $R_2 = 11.9^{+1.4}_{-1.4}$ km (lighter star). These constraints on $R_{1,2}$ were obtained requiring that the EoS supports NS with masses larger than $1.97M_\odot$. Furthermore, the tidal deformability of a $1.4M_\odot$ NS was estimated to be $70 < \Lambda_{1.4M_\odot} < 580$ at the 90% level [14].

The detection of GWs from the GW170817 event was followed by the electromagnetic counterparts, the gamma-ray burst (GRB) GRB170817A [15], and the electromagnetic transient AT2017gfo [16], that set extra constraints on the lower limit of the tidal deformability [17–21]. This last constraint seems to rule out very soft EoS: the lower limit of the tidal deformability of a $1.37M_\odot$ star set by the above studies limits the tidal deformability to $\Lambda_{1.37M_\odot} > 210$ [19], 300 [18], 279 [20], and 309 [21].

Without a reliable theory of dense neutron-rich matter, we depend on different parameterizations to describe the EoS of NS matter. One possibility is characterizing the NS matter by a Taylor expansion around the saturation density of symmetric nuclear matter [22–25]. Motivated by the empirical quadratic isospin-dependent form [26], the EoS of homogeneous nuclear matter is normally characterized by successive derivatives, around saturation density and isospin symmetric matter, of both isoscalar and isovector (symmetry

* marcio.ferreira@uc.pt

† cp@fis.uc.pt

energy) parts. These derivatives are identified as the empirical parameters of nuclear matter at saturation. Despite the great effort to determine their values, both from nuclear experiments and nuclear theories, most of them, mainly the higher order empirical parameters, are still unknown (see [22]). The parametrization of the EoS of nuclear matter via a Taylor expansion around saturation density can be thought of having a dual meaning [24]. When used for describing terrestrial nuclear EoS or predictions of nuclear energy density functional theories, they are Taylor expansions near saturation density and symmetric nuclear matter, while at high densities they are just parameterizations to be constrained by astrophysical observations. The advantage of this kind of parametrization is that they satisfy, by construction, all the known constraints for the nuclear matter EoS near saturation density. Therefore, by exploring the present theoretical/experimental uncertainty on the possible range of the empirical parameters, we will construct a dataset of possible candidates for the EoS of nuclear matter that are thermodynamically consistent, causal, and compatible with astrophysical observations. Distinct EoS parametrizations, such as piecewise-polytropic [27–30], spectral representation [31], and speed of sound [32, 33] are also used.

The main objective of the present study is to understand which is the role of the crust EoS on the information we extract from NS observations. In [34], a set of parameterized EoS based on piecewise polytropes was built. These EoS were fitted to several well known NS EoS, including some with a quark core. For the low density EoS the SLy4 crust was considered and the first polytropic curve was extended to lower densities until the SLy4 EoS was crossed. This approach was followed in other studies [35, 36]. In [23] a cubic spline was built to match the SLy4 crust and core EoS between a crust density of the order of $0.1\rho_0$ and a core density of the order of ρ_0 . The authors have verified that changing the lower limit to the double or the upper limit to half the density would not affect the radius of a low (high) mass star in more than 100m (50m). In this procedure it is always possible to match the crust and core EoS and generate a valid model. In the present study, we will consider three different inner crust EoS, resulting from nuclear models with a very different symmetry energy dependence on the density. For the crust-core transition we will consider a first order phase transition and will apply a Maxwell construction. We are aware that besides the EoS also the crust-core matching approach may have an effect on the NS properties. In this work, we will focus on the dependence of the NS properties on the crust EoS taking the same matching procedure for all the EoS. A complete study that considers both the crust EoS and the matching procedure will be left for the future. However, it has been discussed that the ad-hoc matching of the crust to the core may give rise to thermodynamic inconsistencies as discussed in [37].

The paper is organized as follows. In Sec. II, we introduce the EoS parametrization and the different crusts EoS used in this work. We also detail the procedure of generating our sets composed by possible EoS of nuclear matter in β -equilibrium. The neutron stars properties of each set are analyzed and compared in Sec. III. The impact of the crust EoS on several universal relations among NS properties are explored in Sec. IV, while binary NS quantities are studied in Sec. V. The inference of NS properties from the GW170817 event is carried out in Sec. VI. Finally, the conclusions are drawn in Sec. VII.

II. EOS PARAMETRIZATION

We start from the generic functional form for the energy per particle of homogeneous nuclear matter

$$\mathcal{E}(x, \delta) = e_{\text{sat}}(x) + e_{\text{sym}}(x)\delta^2 \quad (1)$$

with

$$\begin{aligned} e_{\text{sat}}(x) &= E_{\text{sat}} + \frac{1}{2}K_{\text{sat}}x^2 + \frac{1}{6}Q_{\text{sat}}x^3 + \frac{1}{24}Z_{\text{sat}}x^4 \quad (2) \\ e_{\text{sym}}(x) &= E_{\text{sym}} + L_{\text{sym}}x + \frac{1}{2}K_{\text{sym}}x^2 + \frac{1}{6}Q_{\text{sym}}x^3, \\ &+ \frac{1}{24}Z_{\text{sym}}x^4 \quad (3) \end{aligned}$$

where $x = (n - n_0)/(3n_0)$. The baryon density is given by $n = n_n + n_p$ and $\delta = (n_n - n_p)/n$ is the asymmetry, with n_n and n_p being the neutron and proton densities, respectively. This approach of Taylor expanding the energy functional up to fourth order around the saturation density, n_0 , has been applied recently in several works [22, 23, 25, 38].

The empirical parameters can be identified as the coefficients of the expansion. The isoscalar empirical parameters are defined as successive density derivatives of e_{sat} ,

$$P_{is}^k = (3n_0)^k \left. \frac{\partial^k e_{\text{sat}}}{\partial n^k} \right|_{\{\delta=0, n=n_0\}}, \quad (4)$$

whereas the isovector parameters measure density derivatives of e_{sym} ,

$$P_{iv}^k = (3n_0)^k \left. \frac{\partial^k e_{\text{sym}}}{\partial n^k} \right|_{\{\delta=0, n=n_0\}}. \quad (5)$$

The corresponding empirical parameters are then

$$\{P_{is}^0 = E_{\text{sat}}, P_{is}^2 = K_{\text{sat}}, P_{is}^3 = Q_{\text{sat}}, P_{is}^4 = Z_{\text{sat}}\} \quad (6)$$

and

$$\{P_{iv}^0 = E_{\text{sym}}, P_{iv}^1 = L_{\text{sym}}, P_{iv}^2 = K_{\text{sym}}, P_{iv}^3 = Q_{\text{sym}}, P_{iv}^4 = Z_{\text{sym}}\} \quad (7)$$

The coefficients of low orders are already quite well constrained experimentally [39–44], however Q_{sat} , Z_{sat}

and K_{sym} , Q_{sym} , Z_{sym} are only poorly known [23, 24, 45–49]. The saturation energy E_{sat} and saturation density n_0 being rather well constrained, we fix their values throughout this work: $E_{\text{sat}} = -15.8$ MeV (the current estimated value is -15.8 ± 0.3 MeV [22]), and $n_0 = 0.155$ fm^{-3} .

Each possible EoS is represented by a point in the 8-dimensional space of parameters. We use random sampling of models through a multivariate Gaussian with zero covariance:

$$\begin{aligned} \text{EoS}_i &= (E_{\text{sym}}, L_{\text{sym}}, K_{\text{sat}}, K_{\text{sym}}, Q_{\text{sat}}, Q_{\text{sym}}, Z_{\text{sat}}, Z_{\text{sym}})_i \\ &\sim N(\boldsymbol{\mu}, \boldsymbol{\Sigma}) \end{aligned} \quad (8)$$

where

$$\begin{aligned} \boldsymbol{\mu}^T &= (\bar{E}_{\text{sym}}, \bar{L}_{\text{sym}}, \bar{K}_{\text{sat}}, \bar{K}_{\text{sym}}, \bar{Q}_{\text{sat}}, \bar{Q}_{\text{sym}}, \bar{Z}_{\text{sat}}, \bar{Z}_{\text{sym}}) \\ \boldsymbol{\Sigma} &= \text{diag}(\sigma_{E_{\text{sym}}}, \sigma_{L_{\text{sym}}}, \sigma_{K_{\text{sat}}}, \sigma_{K_{\text{sym}}}, \\ &\quad \sigma_{Q_{\text{sat}}}, \sigma_{Q_{\text{sym}}}, \sigma_{Z_{\text{sat}}}, \sigma_{Z_{\text{sym}}}). \end{aligned} \quad (9)$$

In the present approach, as discussed in [23], no a priori correlations exist between the different parameters of the EoS. However, the requirement that every valid EoS must satisfy a set of experimental and observational constraints induces correlations among the parameters in the final set of EoS. The used parameters values and their standard deviations are in Table I.

P_i	E_{sym}	L_{sym}	K_{sat}	K_{sym}	Q_{sat}	Q_{sym}	Z_{sat}	Z_{sym}
\bar{P}_i	32	60	230	-100	300	0	-500	-500
$\sqrt{\sigma_{P_i}}$	2	15	20	100	400	400	1000	1000

Table I. The mean \bar{P}_i and standard deviation $\sqrt{\sigma_{P_i}}$ of the multivariate Gaussian, where σ_{P_i} is the variance of the parameter P_i . Our EoSs are sampled using the initial distribution for P_i assuming that there are no correlations among the parameters. All the quantities are in units of MeV. These values are from [23].

We impose the following conditions to get a valid EoS: i) the pressure is an increasing function of density (thermodynamic stability); ii) the speed of sound is smaller than the speed of light (causality); iii) the EoS supports a maximum mass at least as high as $1.97M_{\odot}$ [1–4] (observational constraint); and iv) the symmetry energy $e_{\text{sym}}(n)$ is positive. This may be a too restrictive constraint and a more realistic would be that the symmetry energy $e_{\text{sym}}(n)$ is positive for densities below the central density of the maximum mass star configuration. We consider, however, that the difference between both sets of EoS will not be significant. All EoS describe $npe\mu$ matter in β -equilibrium.

A. Adding a crust to the generated EoSs

To test the dependence of our results on the crust, we have built three different sets of NS EoS taking three

different crust EoS: the SLy4 [50] and two other EoS obtained from a Thomas Fermi calculation of the inner crust [51–53] taking as underlying models the relativistic mean field (RMF) models NL3 [54], and DDHd [55], respectively with a stiff and a soft symmetry energy EoS above saturation density. It has been discussed in [37, 56] that the inner crust is quite sensitive to the symmetry energy density dependence. Taking the three inner crust EoS, two of them having extreme behaviors of the symmetry energy, will allow us to discuss how sensitive are the results to the crust EoS. In Fig. 1, the pressure is plotted as a function of the baryonic density for these three crusts, and it is clearly seen their different behavior.

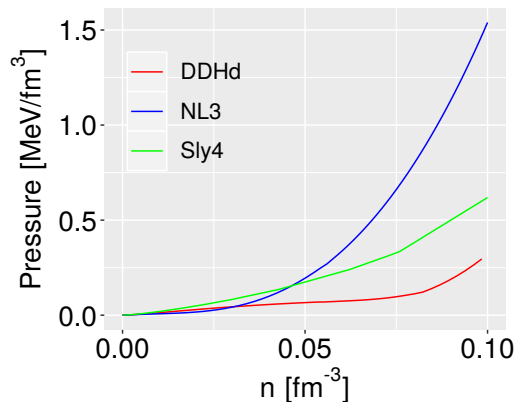


Figure 1. Pressure as a function of density for the DDHd (red), NL3 (blue), and SLy4 (green) crusts.

It has been long discussed in the literature whether the crust-core transition is a first order phase transition or a crossover, see for instance [57, 58] and references therein. Since we are considering a two model approach to determine the complete EoS, one for the crust and the other for the core, a thermodynamic consistent description of the crust-core transition is to consider the Maxwell construction for a first order phase transition. We impose that a valid core EoS must cross one of the above crust EoS in the $P(\mu)$ plane below $n < 0.10$ fm^{-3} , consistently with the range of core-crust transition densities for a large set of nuclear models [59]. The crusts are matched with the generated EoSs by requiring $P_{\text{crust}}(\mu) = P_{\text{core}}(\mu)$, where μ is the baryonic chemical potential. All EoS that do not cross the crust EoS at $n < 0.10$ fm^{-3} are discarded. Our approach is more restrictive than the one proposed in [23], where a cubic spline was chosen as a matching procedure to link the crust and core EoS.

III. THE EOS SET

In this section, we discuss the properties of the EoS sets used in the present study, including the match of the crust EoS to the core EoS. The properties of the NSs built from these sets of EoS and their possible dependence on the examined crusts are summarized.

A. EoS dataset

After matching the crust EoS and applying all the conditions at the end of Sec. II, we ended up with 1956 (DDHd crust EoS), 5167 (NL3 crust EoS), 2158 (SLy4 crust EoS) valid models. In Fig. 2 the histograms of the crust-core matching densities are shown for the three crusts considered. The requirement that the matching has to occur for densities below 0.1 fm^{-3} has a clear effect only for the EoSs built with the NL3 crust. This is due to the fact that being a quite hard crust EoS it is easier that the crust-core matching is successful. The SLy4 EoS shows the lowest mean value for the transition density (blue dashed lines), followed by the DDHd crust, and the NL3 shows the highest value, around 0.08 fm^{-3} .

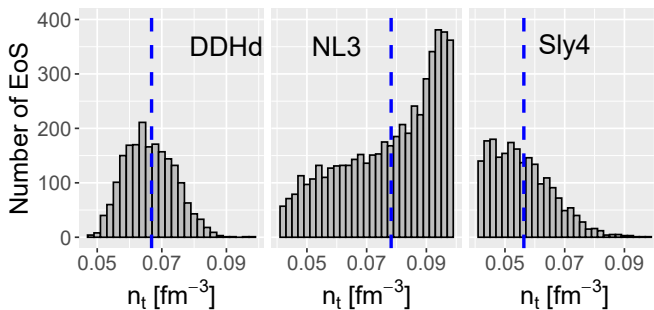


Figure 2. Histograms for the transition density between the generated EoSs and the crusts: DDHd (left), NL3 (middle) and SLy4 (right). The mean values are represented by blue dashed lines.

The mean values and standard deviations for the empirical parameters of our final sets are shown in Table II. The mean values of K_{sat} , E_{sym} , and L_{sym} slightly change when compared to their initial values, indicating that the conditions applied did not require their values to change considerably. As referred in [23], this is probably due to the fact that these parameters are already well constrained and most of the conditions applied probe high densities. It should be noticed, however, that the DDHd crust affects quite strongly the E_{sym} distribution. The effect of the crust on the probability distributions of the EoS parameters is only reflected on the lower order isovector parameters. The third and fourth order parameters Q_i and Z_i are totally insensitive to the crust. This behavior was expectable since these parameters control the high density part of the EoS and the crust slightly affects the high density region of a NS.

B. Neutron stars properties

Using our three sets of EoS, we determine the $M(R)$ relations by integrating the Tolman-Oppenheimer-Volkoff (TOV) equations [60, 61], and the dimensionless tidal

	NL3		DDHd		SLy4	
x_i	\bar{x}	σ_x	\bar{x}	σ_x	\bar{x}	σ_x
E_{sym}	32.32	1.78	28.31	1.00	33.32	1.89
L_{sym}	59.62	10.38	69.59	13.85	51.56	11.83
K_{sat}	230.15	20.08	229.54	21.26	233.95	18.75
K_{sym}	-61.31	70.38	-88.54	80.06	-43.96	63.02
Q_{sat}	75.76	127.64	78.54	132.28	58.62	123.33
Q_{sym}	259.68	310.29	302.01	318.98	238.21	300.33
Z_{sat}	-199.75	145.98	-201.70	147.98	-181.97	143.04
Z_{sym}	348.50	676.47	344.80	719.04	371.91	698.56

Table II. The mean $\bar{x} = (1/N) \sum_i x_i$ and standard deviation $\sigma_x = \sqrt{1/(N-1) \sum_i (x_i - \bar{x})^2}$ of the empirical parameters. Results obtained with the three inner crusts discussed in the text, DDHd, NL3 and SLy4, are shown. All the quantities are in units of MeV.

deformabilities Λ

$$\Lambda = \frac{2}{3} k_2 C^{-5}, \quad (10)$$

where k_2 is the quadrupole tidal Love number (determined following Ref. [62]) and $C = GM/(c^2 R)$ is the star's compactness.

Figure 3 shows the $M(R)$ and $\Lambda(M)$ diagrams for all models (the color distinguishes the crust used). A summary of the mean values and the standard deviations for Λ_{M_i} and R_{M_i} is in Table III. The NL3 and SLy4 crusts show similar results for the mean values and standard deviations, however the NL3 crust shows more extreme values. Matching the generated EoSs with the DDHd crust results in larger and more scattered radii, mainly for low NSs masses.

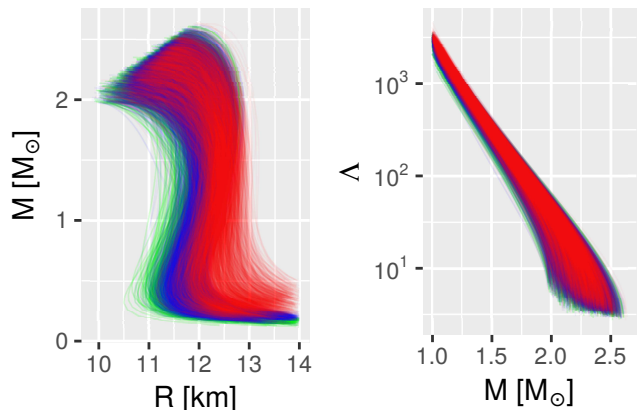


Figure 3. Mass-Radius (left) and Λ -mass (right) diagrams for all valid models with the three different crusts: DDHd (red), NL3 (blue), and SLy4 (green).

From the reanalysis of GW170817 data, assuming the same EoS for the two NSs and for a spin range consistent with the one observed in Galactic binary NSs, the

x_i	NL3		DDHd		SLy4	
	\bar{x}	σ_x	\bar{x}	σ_x	\bar{x}	σ_x
$\Lambda_{1.0M_\odot}$	3073.15	285.07	3323.69	347.94	2978.05	292.00
$\Lambda_{1.2M_\odot}$	1159.03	121.49	1229.02	136.18	1133.65	122.79
$\Lambda_{1.4M_\odot}$	476.89	59.81	498.89	64.55	469.76	59.84
$\Lambda_{1.6M_\odot}$	205.28	32.50	212.68	34.78	203.12	32.32
$\Lambda_{1.7M_\odot}$	88.90	19.02	91.53	20.21	88.18	18.9
$R_{1.0M_\odot}$	12.06	0.18	12.38	0.28	11.97	0.19
$R_{1.2M_\odot}$	12.17	0.19	12.43	0.25	12.10	0.20
$R_{1.4M_\odot}$	12.24	0.21	12.46	0.25	12.18	0.22
$R_{1.6M_\odot}$	12.26	0.25	12.43	0.28	12.21	0.25
$R_{1.8M_\odot}$	12.19	0.32	12.33	0.34	12.15	0.32

Table III. Mean and standard deviation values for Λ_{M_i} and R_{M_i} (km) for the three inner crusts discussed in the text, NL3, DDHd, and SLy4.

tidal deformability of a $1.4M_\odot$ NS was estimated to be $70 < \Lambda_{1.4M_\odot} < 580$ at the 90% level [14]. Almost all EoS in our set are within this interval. Our set of models does not contain models with $\Lambda_{1.4M_\odot} < 200$. However, this is not a drawback since the GRB 170817A [15], and the electromagnetic transient AT2017gfo [16] detected immediately after the GW170817 detection set an extra constraint on the lower limit of the tidal deformability [17, 19–21, 63] ruling out very soft EoS. In particular, the lower limit of the tidal deformability of a $1.37M_\odot$ star imposes $\Lambda_{1.37M_\odot} > 210$ [19], 300 [18], 279 [20], and 309 [21].

IV. UNIVERSAL RELATIONS: NEUTRON STAR PROPERTIES

In the present and following sections, we investigate several relations between NS properties using the set of models defined in the previous sections.

A. Love number k_2

The tidal Love number k_2 is restricted to a narrow range of values, $0.05 \lesssim k_2 \lesssim 0.15$, when considering several hadronic EoS and star masses in the range $1.0 < M/M_\odot < 1.8$. This fact favors the existence of an approximately universal relation between the tidal deformability Λ and the compactness C which was first proposed in [64]. The authors of [65] have discussed this relation and compared with other universal relations relating global properties of NS as the I-Love-Q and I-Love relations [65–67] and have shown that the EoS dependence of the compactness C relation with any of the quantities I-Love-Q is much larger than the variation in the I-Love-Q relations.

Considering a set of three EoS with quite different density dependence, it was found that $C = a_0 + a_1 \ln \Lambda + a_2 (\ln \Lambda)^2$ [64]. A fit using a wider set of EoS was performed in [65] and the maximum deviation obtained was 6.5%. Still, in [68] the tidal deformability was related to the compactness through $\Lambda = a C^{-6}$, where $a = 0.0093 \pm 0.0007$ for stars with a mass in the range $1.1 \leq M/M_\odot \leq 1.6$. The extra C^{-1} dependence was shown to come from the tidal Love number k_2 . The same authors have also verified that Λ varies with M^{-6} . In their study, the crust was described by the BPS [69] and the Negele & Vautherin [70] EoS below a transition density of the order of one fourth of saturation density. In the following, we investigate the effect of the crust on the relation between the tidal deformability and compactness taking our set of EoS.

As k_2 depends on both C and the EoS, a possible relation between the measurable quantity Λ and k_2 may give us insights into the EoS properties. In Fig. 4, k_2 is plotted versus C (left), M (middle), and R (right) for $1.1 \leq M/M_\odot \leq 1.6$, the range of masses covered by the GW170817 event. Within the range of masses $1.0 < M/M_\odot < 1.8$, k_2 reduces to half, $k_2(1.8M_\odot)/k_2(1.0M_\odot) \approx 0.5$, while C doubles, $C(1.8M_\odot)/C(1.0M_\odot) \approx 2$. All crusts give similar mean values and deviations for both C and k_2 . The largest difference between the results obtained for the three crusts lies on the dispersion of the values. It is observed a clear

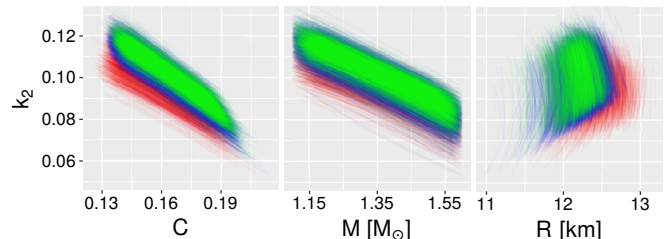


Figure 4. k_2 versus C (left), M (middle), and R (right) for $1.1 \leq M/M_\odot \leq 1.6$ and for each crust: DDHd (green), SLy4 (blue), and NL3 (red).

linear relation between k_2 and C or M . On the other hand, k_2 seems to be insensitive to R . Let us analyze the the two first relations. For the compactness C , we have performed the linear regression $\ln(k_2) = \beta \ln(C) + \alpha$ for each crust EoS. The regression results are

$$[\beta = -1.122, \alpha = -4.358, \text{corr} = 0.933] \text{ NL3} \quad (11)$$

$$[\beta = -1.025, \alpha = -4.244, \text{corr} = 0.860] \text{ DDHd} \quad (12)$$

$$[\beta = -1.137, \alpha = -4.367, \text{corr} = 0.941] \text{ SLy4}, \quad (13)$$

where corr stands for correlation. The correlations are calculated via the Pearson coefficient $\text{Corr}[x, y] = E[(x - \mu_x)(y - \mu_y)]/(\sigma_x \sigma_y)$, where $y = \ln(k_2)$ and $x = \ln(C)$, for the above case. The results indicate that $k_2 \sim C^{-1}$

with a correlation coefficient that is above 90% for the NL3 and the SLy4 crusts. For DDHd the correlation is slightly weaker. The same analysis was repeated for $k_2(M)$ taking the linear regression $\ln(k_2) = \beta \ln(M) + \alpha$. We get

$$[\beta = -1.065, \alpha = -2.006, \text{corr} = 0.892] \text{ NL3} \quad (14)$$

$$[\beta = -1.028, \alpha = -2.061, \text{corr} = 0.843] \text{ DDHd} \quad (15)$$

$$[\beta = -1.069, \alpha = -1.992, \text{corr} = 0.898] \text{ SLy4.} \quad (16)$$

These results indicate that $k_2 \sim M^{-1}$ with a smaller correlation coefficient than the one obtained above, but still as high as 88%-90%, and an exponent deviation from -1 of the order of 5%.

B. Tidal deformability Λ

We next analyze the tidal deformability dependences. Figure 5 shows the diagrams $\Lambda(C)$ (left), $\Lambda(M)$ (middle) and $\Lambda(R)$ (right), for $1.1 \leq M/M_\odot \leq 1.6$. Similarly to k_2 , the crusts do not have a strong impact on the Λ dependences. Performing a similar regression analysis as

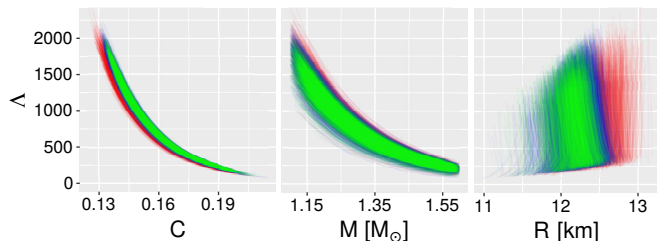


Figure 5. Λ versus C (left), M (right), and R (right) diagrams for $1.1 \leq M/M_\odot \leq 1.6$ for each crust: DDHd (green), SLy4 (blue), and NL3 (red).

above but now for $\Lambda(C)$, i.e., taking $\ln(\Lambda) = \beta \ln(C) + \alpha$, we get

$$[\beta = -6.122, \alpha = -4.763, \text{corr} = 0.998] \text{ NL3} \quad (17)$$

$$[\beta = -6.025, \alpha = -4.649, \text{corr} = 0.995] \text{ DDHd} \quad (18)$$

$$[\beta = -6.137, \alpha = -4.772, \text{corr} = 0.998] \text{ SLy4.} \quad (19)$$

The above results indicate that $\Lambda \sim C^{-6}$ with a high quality fit, similarly to [68], and a small dependence on the crust. The deviation of the exponent from -6 is below 2%. This is expected because $\Lambda(C) \sim k_2(C)C^{-5}$ and we saw that $k_2 \sim C^{-1}$ with the exponent equal to -1 within a deviation below 13%. The values obtained for α are in agreement with $\alpha = -4.6777_{-0.073}^{0.078}$ found in [68].

Let us now analyze the $\Lambda(M)$ dependence through the linear regression $\ln(\Lambda) = \beta \ln(M) + \alpha$. The results are

$$[\beta = -5.962, \alpha = 8.113, \text{corr} = 0.978] \text{ NL3} \quad (20)$$

$$[\beta = -6.055, \alpha = 8.188, \text{corr} = 0.977] \text{ DDHd} \quad (21)$$

$$[\beta = -5.922, \alpha = 8.088, \text{corr} = 0.977] \text{ SLy4} \quad (22)$$

The results indicate that the relation obtained in [68], $\Lambda \sim M^{-6}$, is verified with an exponent slightly different from -6 , the difference not exceeding 4%, and a small dependence on the crust.

On the right panel of Fig. 4 and 5, we also show that the dependence of k_2 and Λ on the star radius. Each EoS appears as a vertical line in both diagrams, because each EoS predicts an almost constant R for $1.1 \leq M/M_\odot \leq 1.6$. This is already seen in the left panel of Fig. 3. We can easily determine the statistics for $\Delta R = R_{1.6M_\odot} - R_{1.1M_\odot}$. The results are $\overline{\Delta R} \pm \sigma = 0.021 \pm 0.185$ km (DDHd), 0.135 ± 0.143 km (NL3), and 0.170 ± 0.140 km (SLy4). Our set of EoS predicts a larger variation of the radius for the NL3 and SLy4 crusts than the study presented in [68], where $\Delta R = 0.070$ km and $\sigma = 0.11$ km were obtained with a set of piece-wise polytrope EoSs. The model with the crust DDHd is the only one compatible with $\Delta R \approx 0$, while the other two models predict $R_{1.6M_\odot} > R_{1.4M_\odot}$ on average.

However, we normally know the mass of a NS, M_i , and we want to infer the Λ_{M_i} from R_{M_i} or the other way around. Fixing the NS mass, we have the relation $\Lambda \sim k_2(R)R^5$, and the dependence $k_2(R)$ should be different from $k_2(C)$. Let us analyze the following empirical relation between the tidal deformability and the radius of a NS with mass M_i ,

$$\Lambda_{M_i} = aR_{M_i}^\beta.$$

In [71], the relation was found to be valid with $\beta = 7.5$ (to a rather good accuracy) for $M_i = 1.4M_\odot$. The authors have explored a sample of 250000 EoS constructed by polytropes segments that interpolate between the EoS obtained from an effective chiral field theory calculation at low density and perturbative QCD results at very high densities. In [72], using a set of relativistic and non-relativistic mean-field models and unified EoS, a value of $\beta = 6.13$ was obtained but the exponent β was seen to be mass dependent: for $M = 1.17$ and $1.6M_\odot$ the values, respectively, $\beta = 5.84$ and 6.58 were determined. In [73], $\beta = 5.28$ was found for $1.4M_\odot$ using several energy density functionals within relativistic mean field (RMF) theory. This relation shows, therefore, some sensitivity to the star mass and to the set of EoS used. The dependence on the set of EoS is probably due to the constraints that have been imposed to build the sets.

In the following, starting from the set of EoS developed for the present study, we explore the same relation and its validity for different NS masses and analyze the impact of the crust. Table IV contains the results of the linear regression $\ln(\Lambda_{M_i}) = \beta \ln(R_{M_i}) + \alpha$ performed for each mass value and each crust and the respective correlation coefficient. As in [72], we see that the exponent β is mass dependent but with a stronger variability. Furthermore, its value depends on the crust used, being its impact stronger for lighter NSs masses. For the canonical NS

mass, both NL3 and SLy4 crusts show very close values, 7.25 and 7.21 respectively, similar to the one obtained in [71], but the DDHd crust predicts a smaller value, 5.81.

For massive NSs, the relation $\Lambda_{M_i} = aR_{M_i}^\beta$ becomes almost exact with a small crust dependence: for $M \geq 1.8M_\odot$ NSs a correlation of 0.99 for NL3 and SLy4 and 0.97 for DDHd was obtained. This almost universal relation shows that the radii of massive neutron stars could be precisely determined from their tidal deformability values. To quantify the uncertainty on R_{M_i} , one can determine the Residual Standard Error (RSE) of the linear regression $R_{M_i}(\Lambda_{M_i})$ that quantifies the dispersion of R_{M_i} around the regression line. We get a RSE(R_{M_i}) of 0.08 km and 0.05 km for $M_i = 1.0M_\odot$ and $M_i = 1.9M_\odot$, respectively, using the NL3 crust.

M_i	α			β			Correlation		
	NL3	SLy4	DDHd	NL3	SLy4	DDHd	NL3	SLy4	DDHd
1.0	-6.14	-6.90	-2.02	5.69	6.00	4.02	0.89	0.93	0.84
1.2	-9.23	-9.35	-4.98	6.51	6.57	4.80	0.93	0.95	0.84
1.4	-12.19	-11.97	-8.89	7.33	7.25	5.98	0.95	0.96	0.88
1.6	-14.94	-14.65	-13.08	8.08	7.97	7.31	0.97	0.98	0.93
1.8	-17.56	-17.40	-16.74	8.81	8.75	8.45	0.99	0.99	0.97
1.9	-18.90	-18.82	-18.38	9.19	9.16	8.95	0.99	0.99	0.98

Table IV. Results for the linear regression $\ln(\Lambda_{M_i}) = \beta \ln(R_{M_i}) + \alpha$ and respective correlation coefficient for the three crust EoS. M_i are in units of M_\odot .

We conclude that not only the relation $\Lambda \sim R^\beta$ depends on the NS mass but also on the crust. The correlation becomes stronger as the NS mass increases and for $1.6M_\odot$ the relation $\Lambda \sim R^\beta$ is almost an exact power law. In a sense, this is telling us that k_2 only behaves as a power law for massive NSs. Clearly, the k_2 has a non-trivial dependence on R that changes with the NS mass being considered. In fact, for a fixed mass, k_2 is by no means a power law in R . This becomes the case, only in an approximate way, for $M \geq 1.6M_\odot$. The regression analysis results using the relation $\ln(k_2) = \beta \ln(R_M) + \alpha$ are show in Table V. It is striking that for $M \geq 1.8M_\odot$ the correlation is 0.99 for the crusts NL3 and SLy4. In [72], the authors have also shown that with a set of 33 RMF and Skyrme EoS there was a reasonable correlation between k_2 and R for a $1.4M_\odot$ star. With our set, we get a weaker correlation for a $1.4M_\odot$ star but we show that the larger the NS mass the stronger the correlation.

To conclude this section, we summarize the main results: a) we confirm the results presented in [68] concerning the relations $\Lambda(C)$ and $\Lambda(M)$, in particular, that $\Lambda \sim C^{-6}$ and $\Lambda \sim M^{-6}$ is obtained with a high quality fit, a deviation of the exponent from -6 , respectively of $\approx 2\%$ and $\approx 4\%$, and a small dependence on the crust; b) for a fixed NS mass M_i , the relation $\Lambda \sim R^\beta$ depends on the crust and on the NS mass. The correlation becomes stronger as the NS mass increases and for $M > 1.6M_\odot$ the relation $\Lambda \sim R^\beta$ is almost an exact power law with

M_i	α			β			Correlation		
	NL3	SLy4	DDHd	NL3	SLy4	DDHd	NL3	SLy4	DDHd
1.0	-3.60	-4.39	0.31	0.60	0.93	-0.98	0.22	0.39	-0.37
1.2	-5.72	-5.94	-1.64	1.41	1.51	-0.24	0.50	0.60	-0.08
1.4	-7.87	-7.76	-4.69	2.21	2.17	0.91	0.72	0.76	0.28
1.6	-10.00	-9.81	-8.18	2.99	2.92	2.23	0.86	0.87	0.62
1.8	-12.11	-12.00	-11.30	3.74	3.71	3.39	0.94	0.94	0.85
1.9	-13.22	-13.18	-12.71	4.14	4.13	3.91	0.96	0.96	0.91

Table V. Parameters of the linear regression, $\ln(k_2) = \beta \ln(R_M) + \alpha$, and respective correlation coefficient. M_i are in units of M_\odot .

$\beta \sim 8 - 9$, and crust independent.

V. BINARY NEUTRON STARS

In this section, we study the impact of the crust on several relations between binary quantities and the properties of the individual NS in the binary.

The leading tidal parameter of the gravitational-wave signal of a NS merger depends on the effective tidal deformability of the binary system

$$\tilde{\Lambda} = \frac{16}{13} \frac{(12q + 1)\Lambda_1 + (12 + q)q^4\Lambda_2}{(1 + q)^5}, \quad (23)$$

where $q = M_2/M_1 < 1$ is the binary mass ratio and $\Lambda_1(M_1)$ and $\Lambda_2(M_2)$ represent the tidal deformability (mass) of the primary and the secondary NS in the binary, respectively. The GW170817 event provides an upper bound of $\tilde{\Lambda} = 300_{-230}^{+420}$ (using a 90% highest posterior density interval and the waveform model PhenomPNRT, although other models may predict a larger upper bound) for the low spin-prior [13]. The binary mass ratio, for the GW170817 event, is bounded as $0.73 \leq q \leq 1$ [13].

The chirp mass of the binary system is another quantity that is measured with a good accuracy during the gravitational wave detection. It is given by

$$M_{\text{chirp}} = \frac{(M_1 M_2)^{3/5}}{(M_1 + M_2)^{1/5}} = M_1 \frac{q^{3/5}}{(1 + q)^{1/5}}. \quad (24)$$

For the GW170817 event, it was measured to be $M_{\text{chirp}} = 1.188_{-0.002}^{+0.004} M_\odot$ [12], and more recently updated to $1.186_{-0.001}^{+0.001} M_\odot$ [13].

A. Relation between $\tilde{\Lambda}$ and $\Lambda_{1,2}$

If the chirp mass expression (Eq. (24)) is rewritten as $M_1(M_{\text{chirp}}, q)$, the binary mass ratio q determines both

M_1 and M_2 for a fixed M_{chirp} . Knowing the binary NS masses, their tidal deformabilities $\Lambda_{1,2}$ and the effective tidal deformability of the binary $\tilde{\Lambda}$ can be determined. In Fig. 6, taking the GW170817 chirp mass, $M_{\text{chirp}} = 1.186M_{\odot}$, we show the tidal deformability of each star $\Lambda_{1,2}$ as a function of the binary tidal deformability $\tilde{\Lambda}$ for three representative values of the binary mass ratio q : 0.947, 0.826, 0.729. Since we have shown that $\Lambda_{1,2} \sim M_{1,2}^{-6}$ in Sec. IV, we get $\Lambda_2 \sim q^{-6}\Lambda_1$. As expected, when the binary mass ratio q decreases, it is the lighter NS tidal deformability Λ_2 that dominates $\tilde{\Lambda}$ and, therefore, the correlation is stronger for the star M_2 . This is clearly seen when comparing the top and bottom right panels of Fig. 6. For almost symmetrical binary systems, as the $(1.40 M_{\odot}, 1.33 M_{\odot})$ system, $q \approx 1$, we have $M_1 \approx M_2$ and $\Lambda_2 \approx \Lambda_1 \approx \Lambda$, which leads to $\tilde{\Lambda} \propto \Lambda$ (see left panels of Fig. 6).

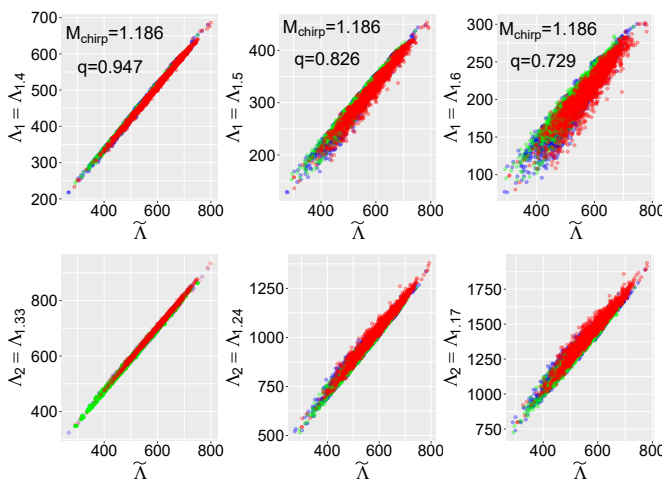


Figure 6. The effective binary tidal deformability $\tilde{\Lambda}$ versus the tidal deformability of each component stars $\Lambda_{1,2}$ for several values of the binary mass ratio, $q = 0.947$ (left), $q = 0.826$ (middle), and $q = 0.729$ (right), and for a fixed chirp mass of $M_{\text{chirp}} = 1.186M_{\odot}$. The different crusts EoS are shown: DDHd (red), NL3 (green), and SLy4 (blue).

Let us consider the binary mass ratio $q = 0.947$ (left panels in Fig. 6), and analyze what information can be extracted from $\tilde{\Lambda}$ on $\Lambda_1 = \Lambda_{1.4M_{\odot}}$ (the heavier NS component of the binary). Doing the linear regression $\Lambda_{1.4M_{\odot}} = \beta\tilde{\Lambda} + \alpha$, we obtain

$$[\beta = 0.884, \alpha = -18.807, \text{corr} = 0.998] \text{ NL3} \quad (25)$$

$$[\beta = 0.881, \alpha = -18.857, \text{corr} = 0.998] \text{ DDHd} \quad (26)$$

$$[\beta = 0.882, \alpha = -16.847, \text{corr} = 0.999] \text{ SLy4} \quad (27)$$

The regression results are similar for all crusts and show very strong correlations, and, consequently, $\Lambda_{1.4M_{\odot}}$ can be accurately extracted from $\tilde{\Lambda}$. In [48], the authors have obtained $\beta = 0.859$ also with a very large correlation coefficient, using a set of relativistic and non-relativistic mean-field models. This seems to indicate

that $\Lambda_{1.4M_{\odot}}(\tilde{\Lambda})$ relation is quite insensitive to the EoS parametrization used.

B. Relation between $\tilde{\Lambda}$ and $R_{1,2}$

Let us now study the relation between the effective tidal deformability $\tilde{\Lambda}$ and $R_{1,2}$. In [74, 75], the authors have looked at this problem taking six nuclear EoS and obtained a strong correlation between $\tilde{\Lambda}$ and R_1 , which showed to be quite independent of the individual component masses. From this correlation they could conclude that an upper bound $\tilde{\Lambda} = 800$ would exclude radii above ~ 13 km at the 90% confidence level. In the following we examine this same problem with our set of EoS and check how strongly is it affected by the crust.

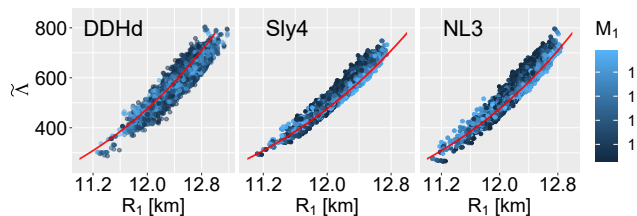


Figure 7. $\tilde{\Lambda}$ as a function of R_1 by fixing the $M_{\text{chirp}} = 1.186M_{\odot}$. The red curves in three panels are the fit proposed in [74, 75].

In Fig. 7, we plot the $\tilde{\Lambda}$ as a function of the radius of the primary NS in the binary, R_1 , for $M_{\text{chirp}} = 1.186M_{\odot}$ and $0.73 < q < 1.0$. All three crusts are shown: DDHd (left), NL3 (middle) and SLy4 (right). Our set of EoS only describes $\tilde{\Lambda} < 800$ values, however the plot confirms that there is a strong correlation between $\tilde{\Lambda}$ and R_1 that is not destroyed by the individual component masses. A plot of the $\tilde{\Lambda}$ versus the radius of the secondary NS in the binary, R_2 , would give the same results. The red curve in these panels represents the fit proposed in [74, 75]. Although the correlation between the effective tidal deformability and R_1 is strong, we conclude that it is crust dependent and the fitting curve depends on the EoS set, SLy4 giving the strongest correlation.

Performing the linear regression $\ln(\tilde{\Lambda}) = \beta \ln(R_1) + \alpha$, we get

$$[\beta = 6.554, \alpha = -10.108, \text{corr} = 0.966] \text{ NL3} \quad (28)$$

$$[\beta = 5.729, \alpha = -8.083, \text{corr} = 0.926] \text{ DDHd} \quad (29)$$

$$[\beta = 6.553, \alpha = -10.093, \text{corr} = 0.973] \text{ SLy4} \quad (30)$$

The crust has an impact of the order $\approx 14\%$ on the exponent that describes the dependence of $\tilde{\Lambda}$ on R_1 , when the only constraint set on the star mass is that $0.73 < M_2/M_1 < 1.0$ and $1.1 < M/M_{\odot} < 1.6$.

C. Relation between $\tilde{\Lambda}$ and M_{chirp}

We next analyze the impact of M_{chirp} on $\tilde{\Lambda}$. From Eq. (23), the effective tidal deformability of the binary, $\tilde{\Lambda}$, is written as a function of q and M_{chirp} , $\tilde{\Lambda}(M_{\text{chirp}}, q)$. In Fig. 8, $\tilde{\Lambda}$ is plotted as a function of q for a fixed $M_{\text{chirp}} = 1.186M_{\odot}$ (left) and as a function of M_{chirp} for a fixed $q = 0.90$ (right). We display both the average values (solid lines) and dispersion (shaded region corresponds to $\pm 2\sigma$). Each set with a different crust EoS is represented by a different color. The mean value of $\tilde{\Lambda}$ is quite insensitive to the value of q , as previously discussed in [36], with the DDHd pushing the whole distribution to higher values of $\tilde{\Lambda}$. However, as also shown in [36], the $\tilde{\Lambda}(M_{\text{chirp}})$ dependence for fixed q is strongly dependent on the binary chirp mass M_{chirp} , as shown on the right panel of Fig. 8 for $q = 0.9$. We further conclude that the impact of the crust on these results is small.

To quantify the differences imposed by each crust, we perform the linear regression $\ln(\tilde{\Lambda}) = \beta \ln(M_{\text{chirp}}) + \alpha$. The results are

$$[\beta = -5.824, \alpha = 7.312, \text{corr} = -1.000] \text{ NL3} \quad (31)$$

$$[\beta = -5.910, \alpha = 7.375, \text{corr} = -1.000] \text{ DDHd} \quad (32)$$

$$[\beta = -5.781, \alpha = 7.288, \text{corr} = -1.000] \text{ SLy4}, \quad (33)$$

which indicate that $\tilde{\Lambda}$ and M_{chirp} are highly correlated. Moreover, we get a similar dependence as the one discussed in [68], where $\tilde{\Lambda} \sim M_{\text{chirp}}^{-6}$ was determined, with a exponent about 3% smaller. The above results are only slightly dependent on the crust.

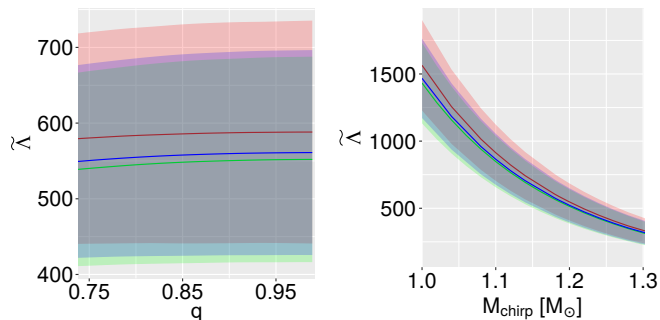


Figure 8. $\tilde{\Lambda}$ density as a function of q by fixing the $M_{\text{chirp}} = 1.186M_{\odot}$ (left) and as a function of M_{chirp} by fixing $q = 0.90$ (right). The solid lines represent the mean values and the shaded region encloses $\pm 2\sigma$ for DDHd (blue), SLy4 (red), and NL3 (black) crusts.

D. Relation $\Lambda_1/\Lambda_2 = q^a$ and dependence on M_{chirp}

In [68], a reanalysis of the GW170817 event was made, assuming the relation $\Lambda_1/\Lambda_2 = q^6$, based on the assumption that the two stars of the binary have the same EoS. The above relation was a consequence of two empirical

relations $R_1 \approx R_2$ (for $1.1 \leq M/M_{\odot} \leq 1.6$) and $\Lambda \sim C^6$ within the EoS piecewise-polytrope methodology [68]. In Sec. IV, from the regression analysis of $\Lambda(M)$ (see Fig. 5), we got $\Lambda \sim C^a$ with $a = \{-6.122, -6.025, -6.137\}$, for the NL3, DDHd, and SLy4 crusts, respectively, with an almost perfect correlation ($\text{corr} \approx 1$). Let us recall that, as shown in Sec. IV, only the model with the crust DDHd gives results compatible with $\Delta R = R_{1.6M_{\odot}} - R_{1.1M_{\odot}} \approx 0$.

To test the relation $\Lambda_1/\Lambda_2 = q^a$, we determine the linear regression $\ln(\Lambda_1/\Lambda_2) \sim a \ln(q)$ for a given M_{chirp} . In Fig. 9 left panel, we show the mean value of a , the $\pm\sigma$ deviation, and the minimum/maximum values as a function of M_{chirp} . The correlation value (right panel) shows that the relation $\ln(\Lambda_1/\Lambda_2) \sim a \ln(q)$ perfectly captures the dependence between Λ_1/Λ_2 and q . The exponent a is an increasing function of M_{chirp} . However, there is a considerable spread, and the standard deviation is always larger than 0.5 and gets larger with increasing M_{chirp} . Some EoS show a values that deviate more than 38% from the mean value (dashed lines). We have obtained $5.25 < a < 6.91$ for $1.0 \leq M_{\text{chirp}}/M_{\odot} \leq 1.3$, and including the uncertainty that is attributed to the crust. Considering only the SLy4 crust, this interval would reduce to $5.25 < a < 6.68$. In [68], in a similar study the authors have obtained $5.76 < a < 7.48$. Although not very different, our results correspond to larger values of the ratio Λ_1/Λ_2 , up to 50% (15%) larger at the lower (upper) limit.

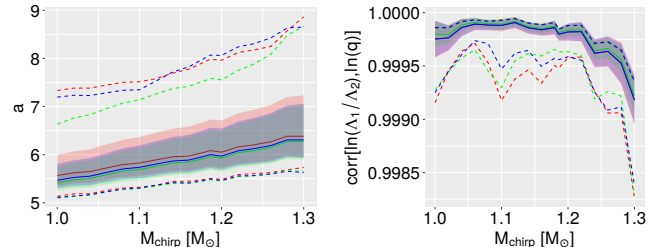


Figure 9. Dependence of a (left) and $\text{Corr}[\ln(\Lambda_1/\Lambda_2), \ln(q)]$ (right) on M_{chirp} (in units of M_{\odot}). It is shown the mean value (solid line), $\pm\sigma$ region (shaded region), and minimum/maximum values (dashed lines). The results for all crust are shown: NL3 (green), SLy4 (red), and DDHd (blue).

We have further studied the dependence of the exponent a , the solid lines in Fig. 9 left panel, on the chirp mass M_{chirp} . Performing the linear regression $\ln(\bar{a}) = \beta \ln(M_{\text{chirp}}) + \alpha$, where \bar{a} represents the mean value of the exponent a , we have obtained

$$[\beta = 0.551, \alpha = 1.696, \text{corr} = 0.996] \text{ NL3} \quad (34)$$

$$[\beta = 0.528, \alpha = 1.714, \text{corr} = 0.926] \text{ DDHd} \quad (35)$$

$$[\beta = 0.564, \alpha = 1.687, \text{corr} = 0.996] \text{ SLy4}. \quad (36)$$

The regression values for β of ≈ 0.5 show that $a \sim \sqrt{M_{\text{chirp}}}$, to a very good approximation. Besides, the correlation obtained with the SLy4 and NL3 crusts is very strong, close to 1.

VI. ESTIMATION OF NS PROPERTIES FROM $\tilde{\Lambda}$

In the present section, the full information from regression analysis will be used in predicting NS properties from GW observables.

Since $\tilde{\Lambda}$ and M_{chirp} are both extractable from gravitational wave detections, it is convenient to analyze what information $\tilde{\Lambda}$ contains about a given NS. In the following, we focus on the GW170817 event, i.e., we fix $M_{\text{chirp}} = 1.186M_{\odot}$, and analyze what we can infer about the tidal deformability and the radius of a NS.

A. Tidal deformability of a $1.4M_{\odot}$ NS

We first analyze the tidal deformability of a $1.4M_{\odot}$ NS. Figure 10 shows $\Lambda_{1.4M_{\odot}}$ vs. $\tilde{\Lambda}$ (top panels) and respective scaled residual (bottom panels) for $q = 0.947$ (left), 0.826 (center), and 0.729 (right).

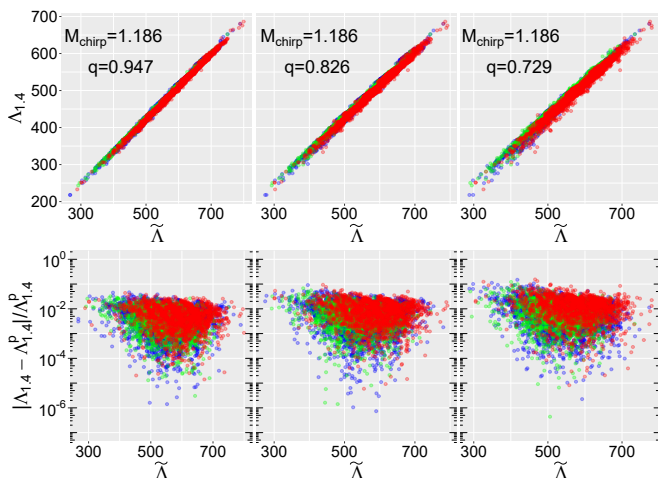


Figure 10. $\Lambda_{1.4M_{\odot}}$ vs. $\tilde{\Lambda}$ (top panels) for different binary mass ratio values: 0.948 (left), 0.826 (center), and 0.729 (right), with fixed $M_{\text{chirp}} = 1.186M_{\odot}$. We also show the respective scaled residuals $(\Lambda_{1.4M_{\odot}} - \Lambda_{1.4M_{\odot}}^p)/\Lambda_{1.4M_{\odot}}^p$ (bottom panels), where $\Lambda_{1.4M_{\odot}}^p$ are the linear regression model predictions (see text). The different crust EoS are shown: DDHd (red), NL3 (green), and SLy4 (blue).

Performing the same linear regression as done for $q = 0.947$ in Eqs. (25)-(27), for $\Lambda_{1.4M_{\odot}} = \beta\tilde{\Lambda} + \alpha$, we get for $q = 0.823$ (middle plot of Fig. 10),

$$[\beta = 0.902, \alpha = -25.278, \text{corr} = 0.997] \text{ NL3} \quad (37)$$

$$[\beta = 0.895, \alpha = -24.780, \text{corr} = 0.995] \text{ DDHd} \quad (38)$$

$$[\beta = 0.901, \alpha = -22.797, \text{corr} = 0.998] \text{ SLy4}, \quad (39)$$

and for $q = 0.729$ (right plot of Fig. 10),

$$[\beta = 0.938, \alpha = -37.374, \text{corr} = 0.994] \text{ NL3} \quad (40)$$

$$[\beta = 0.923, \alpha = -35.053, \text{corr} = 0.989] \text{ DDHd} \quad (41)$$

$$[\beta = 0.936, \alpha = -33.375, \text{corr} = 0.995] \text{ SLy4}. \quad (42)$$

Regardless of the binary mass ratio q , there is always a strong linear relation between $\tilde{\Lambda}$ and $\Lambda_{1.4M_{\odot}}$. The regression analysis shows that both NL3 and SLy4 crusts have similar results while the DDHd predicts a smaller slope value β . Increasing the asymmetry of the binary systems $q < 1$ (i.e., $M_1 > M_2$), the slope increases and there is a decrease on the correlation coefficient. Thus, the higher is the binary asymmetry q the less information $\tilde{\Lambda}$ carries about a $1.4M_{\odot}$ NS.

The scaled residuals of the linear regressions, $(\Lambda_{1.4M_{\odot}} - \Lambda_{1.4M_{\odot}}^p)/\Lambda_{1.4M_{\odot}}^p$, where the $\Lambda_{1.4M_{\odot}}^p$ are the linear regression predictions, are shown in the bottom panels of Fig. 10. The regression $\Lambda_{1.4M_{\odot}}^p = \beta\tilde{\Lambda} + \alpha$ has an overall uncertainty below 5% for $q = 0.947$, while it is around 10% for lower q values. If we consider the extreme lower bound of $q = 0.73$ from [14], we can infer the value of $\Lambda_{1.4M_{\odot}}$ with an 10% accuracy. The precision gets better as one increases the mass ratio value q . This shows that even if a $1.4M_{\odot}$ NS is not part of the binary, it is still possible to determine its tidal deformability, $\Lambda_{1.4M_{\odot}}$, with an accuracy of at least $\sim 10\%$. For the case of the GW170817, the closer the ratio q to one the larger is the accuracy. This is the case because $q = 1$ corresponds to two stars with a mass $1.37M_{\odot}$ very close to $1.4M_{\odot}$. On the other hand, the smaller q the larger the mass difference between both stars, and this blurs to some extent the information that can be drawn from $\tilde{\Lambda}$.

B. Constraining Λ_{M_i} from $\tilde{\Lambda}$

In this section we study the correlation between $\tilde{\Lambda}$ and Λ_{M_i} , i.e. we calculate $\text{Corr}[\Lambda_{M_i}, \tilde{\Lambda}]$, for different NS masses as a function of the binary mass ratio q , in order to answer the question what can we learn from the $\tilde{\Lambda}$ about NSs that have a mass different from $1.4M_{\odot}$.

The results for $M_{\text{chirp}} = 1.186M_{\odot}$ are in Fig. 11 for the NL3 crust (the results are similar for the other two crusts). A strong correlation is found between $\tilde{\Lambda}$ and any Λ_{M_i} with $1.1 < M_i/M_{\odot} < 1.6$. However, depending on the q value, the strongest constraint linearly extractable from $\tilde{\Lambda}$ is either for $\Lambda_{1.3M_{\odot}}$ or for $\Lambda_{1.4M_{\odot}}$. $\tilde{\Lambda}$ contains more information on NS with these masses because they are the intermediate masses for the two extremes defined by q .

This analysis may be used to constrain Λ_{M_i} from observational bounds on $\tilde{\Lambda}$. Our sample does not describe large $\tilde{\Lambda}$ values: for $q = 0.947$ it predicts $\langle \tilde{\Lambda} \rangle \pm 2\sigma = 560.67 \pm 135.11$. However, the strong correlation $\text{Corr}[\Lambda_{M_i}, \tilde{\Lambda}]$ indicates a universal behavior that we can explore to extract constraints on Λ_{M_i} from any observational bound on $\tilde{\Lambda}$.

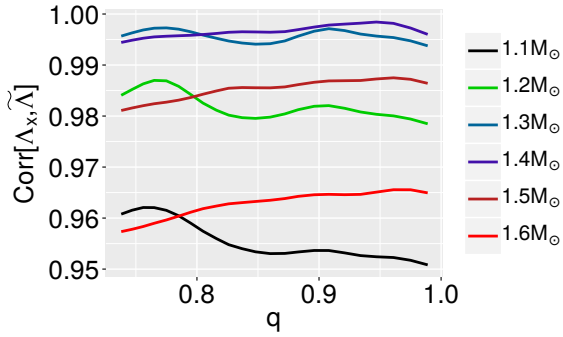


Figure 11. $\text{Corr}[\Lambda_{M_i}, \tilde{\Lambda}]$ as a function of q for $M_i/M_\odot = 1.1, 1.2, 1.3, 1.4, 1.5,$ and 1.6 using the NL3 crust.

In the following, we use first the LIGO/Virgo upper bound $\tilde{\Lambda} = 720$ obtained from the waveform model PhenomPNRT[13] to set an upper bound on Λ_{M_i} as a function of q . Taking next the constraint $\tilde{\Lambda} \geq 300$ [63] obtained from the electromagnetic (EM) counterpart of the GW170817 event, the AT2017gfo/GRB 170817A, we will also derive a lower bound. Although $\tilde{\Lambda}$ does not depend much on q , as shown before (see Fig. 8), Λ_{M_i} is q dependent.

Figure 12 shows the upper bound on $\Lambda_M(q)$ for each crust EoS from the $\tilde{\Lambda} = 720$ constraint. The predictions $\Lambda_M(q)$ for both NL3 and SLy4 crusts are similar. For $M > 1.4M_\odot$, the DDHd predicts higher values than the other two crusts while the opposite happens for higher M values. The width of the confidence intervals reflects the strength of $\text{Corr}[\Lambda_{M_i}, \tilde{\Lambda}]$ displayed in Fig. 11. Λ_M decreases when q increases, due to the β dependence on q . We found, from the regression analysis on $\Lambda_{M_i} = \beta\tilde{\Lambda} + \alpha$ (see Eqs. (25)-(27), (37)-(39), and (40)-(42) for the case of $M_i = 1.4M_\odot$) that β decreases as q grows. This is an indirect effect of the fact that $\tilde{\Lambda}$ increases slightly when q increases, see Fig. 8.

The values of $\Lambda_{1.4M_\odot}(q, \tilde{\Lambda} = 720)$ for the extreme values of q are shown in Table VI (Appendix A). The predictions lie between 636 at $q = 0.74$ and 617 at $q = 0.99$ for the NL3 crust (SLy4 gives slightly higher values), while it is 628 at $q = 0.74$ and 614 at $q = 0.99$ for the DDHd crust. We, therefore, get as an upper bound $\Lambda_{1.4M_\odot} < 640$ at 95% confidence interval, already taking into account the crust effect, that brings an uncertainty not larger than 1%, and the q dependence which brings an uncertainty below 3%.

Table VI also contains a possible lower bound on $\Lambda_{M_i}(q, \tilde{\Lambda})$, for $q = 0.74$ and 0.99 , by using the constraint $\tilde{\Lambda} = 300$ [63] obtained from the electromagnetic (EM) counterpart of the GW170817 event. In this case, the lower bound on $\Lambda_{1.4M_\odot}$ would be $\Lambda_{1.4M_\odot} < 240$ at 95% confidence interval including the crust and q dependence uncertainties.

Taking the above upper and lower bound constraints, we have obtained $240 < \Lambda_{1.4M_\odot} < 640$. This prediction

is compatible with results from other studies. Assuming a common EoS for the two NSs in the binary, the LIGO/Virgo collaborations constrained $70 < \Lambda_{1.4M_\odot} < 580$ at the 90% level [14]. This constraint was obtained without requiring that the EoS should support NSs up to at least $1.97M_\odot$. A higher upper bound on $\Lambda_{1.4M_\odot}$ is expected by requiring that the EoS should comply with massive stars due to the positive correlation between Λ_{M_i} and the maximum NS mass.

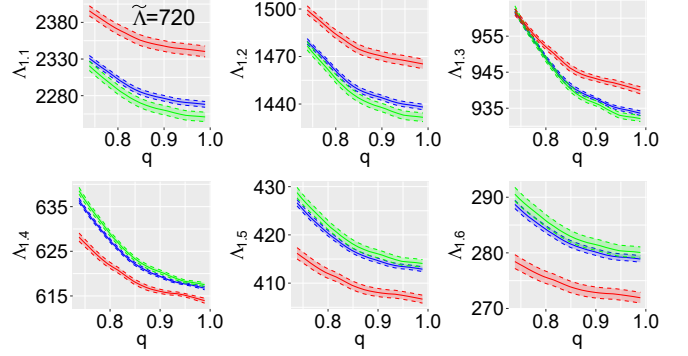


Figure 12. Prediction for $\Lambda_{M_i}(q, \tilde{\Lambda} = 720)$ for $M_i = 1.1, 1.2, 1.3, 1.4, 1.5,$ and $1.6M_\odot$. The solid lines indicates the prediction value while the shaded region represents the 95% confidence interval region. The results for the three crusts are shown: NL3 (blue), SLy4 (red), and DDHd (green).

C. Constraining R_{M_i} from $\tilde{\Lambda}$

We perform a similar analysis of $\text{Corr}[\Lambda_{M_i}, \tilde{\Lambda}]$, but this time on $\text{Corr}[R_{M_i}, \tilde{\Lambda}]$. In this way, we are able to constrain the NS radius for any NS mass. The results are given in Fig. 13, showing that the correlations $\text{Corr}[R_{M_i}, \tilde{\Lambda}]$ are weaker than $\text{Corr}[\Lambda_{M_i}, \tilde{\Lambda}]$ (see Fig. 11). This indicates that Λ_{M_i} has a stronger linear dependence on $\tilde{\Lambda}$ than on R_{M_i} . The $1.4M_\odot, 1.5M_\odot,$ and $1.6M_\odot$ NS are the ones that show the strongest correlations, above 0.95.

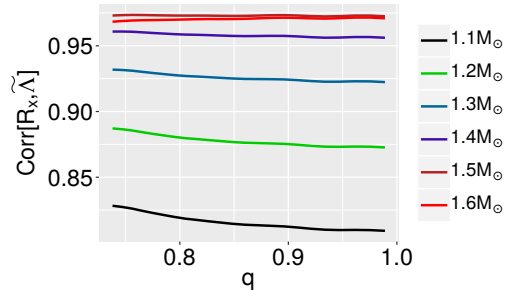


Figure 13. $\text{Corr}[R_{M_i}, \tilde{\Lambda}]$ as a function of q for $M_i = 1.1, 1.2, 1.3, 1.4, 1.5,$ and $1.6M_\odot$ using the NL3 crust.

In Fig. 14, we show the upper bound on R_{M_i} for $M_i = 1.1, 1.2, 1.3, 1.4, 1.5,$ and $1.6M_\odot$ using the LIGO/Virgo

upper bound $\tilde{\Lambda} = 720$ [13]. The predicted value for the radius decreases when q increases. Results obtained for $R_M(q, \tilde{\Lambda} = 720)$ with the NL3 and SLy4 crust are compatible with each other. However, DDHd crust predicts larger radii: a difference that can be as large as $\sim 300\text{m}$ for $M = 1.1M_\odot$, but that reduces to $\sim 50\text{m}$ for $M = 1.6M_\odot$.

The upper bound predictions obtained for the $1.4M_\odot$ star radius, $R_{1.4M_\odot}^{\text{upper}}(q, \tilde{\Lambda} = 720)$, are given in Table VII (Appendix A) for the extreme values of q . They lie between 12.78 km at $q = 0.74$ and 12.71 km at $q = 0.99$ for the NL3 crust and within 0.01 km for the SLy4 crusts. The q dependence introduces an uncertainty of the order of 0.5%. For the DDHd crust, $R_{1.4M_\odot}^{\text{upper}}$ is at least 100 m larger. All the values obtained are compatible with $R = 11.9 \pm 1.4$ km (at the 90% credible level) of the LIGO/Virgo collaborations [14], and also with maximum value $R_{1.4M_\odot} = 13.6$ km reported in [71], where a generic family of EoS interpolating between chiral effective field theory results (low densities) and perturbative QCD (high densities) was used. Our results are also consistent with a mean value of $R_{1.4M_\odot} = 12.39$ km and a 2σ confidence of $12.00 < R_{1.4M_\odot}/\text{km} < 13.45$ in [76], where a piecewise polytrope parametrization of the EoS, which took into account nuclear matter calculations of the outer crust and close to the saturation density, as well as perturbative QCD at very high densities.

Considering the lower bound defined by $\tilde{\Lambda} = 300$, we obtain $R_{1.4M_\odot}^{\text{lower}} > 11.39$ km. In this limit the three crusts predict slightly different radii, with SLy4 predicting the smallest values and DDHd the largest ones.

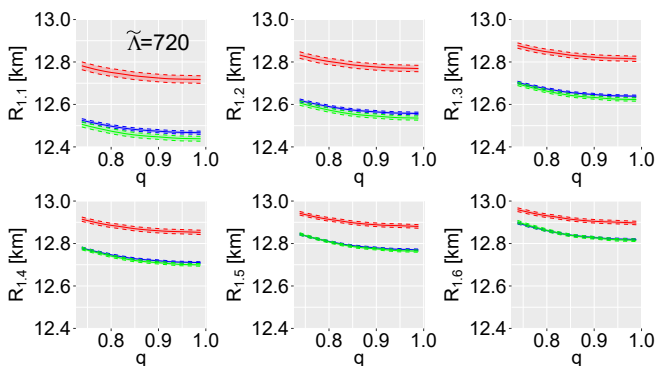


Figure 14. Prediction for $R_{M_i}(q, \tilde{\Lambda} = 720)$ for $M_i = 1.1, 1.2, 1.3, 1.4, 1.5,$ and $1.6M_\odot$. The solid lines indicates the prediction value while the shaded region represents the 95% confidence interval region. The results for the three crusts are shown: NL3 (blue), SLy4 (red), and DDHd (green).

VII. CONCLUSIONS

We have analyzed the impact of the crust EoS on several empirical relations. We have used three sets of EoS in our analyzes, each set with a different inner crust.

The core EoS was determined from a Taylor expansion of the energy functional around the saturation density, n_0 , until fourth order, and different models were generated through random sampling of the empirical parameters via a multivariate Gaussian with zero covariance. Thermodynamic stability, causality, a maximum star mass of $1.97 M_\odot$ and a positive symmetry energy were the conditions imposed to validate the generated EoS. For the crust EoS, we have considered the crusts determined within the models SLy4, NL3 and DDHd, characterized by a quite different density dependence of the symmetry energy at sub-saturation densities. The matching of the crust was imposed to occur below 0.1 fm^{-3} and it was required that the crust and the core pressures are the same at the transition baryonic chemical potential, i.e., a first order phase transition was considered. This matching procedure gives an EoS that is thermodynamically consistent. While other matching procedures are frequently used, and although we left for future work a complete study that considers both the crust EoS and the matching procedure, preliminary results show that the matching procedure only has a very weak impact. The three sets of EoS satisfy the constraints obtained from the analysis of the GW170817 event [13].

First, the relations between the tidal deformability Λ and compactness C , Love number k_2 and radius R_{M_i} were studied. It was shown that $k \propto C^\beta$ with $\beta \approx -1$ for $1.1 \leq M/M_\odot \leq 1.6$, where the crust shows an impact of the order of 11%. The same behavior is found for $k_2(M)$, i.e., $k_2 \propto 1/M$, but with a much smaller impact of the crust, 4%. As a consequence, it was established a correlation of almost one between the compactness C and Λ via the dependence $\Lambda \propto C^\beta$ with $\beta = -6.122, -6.025,$ and -6.137 for the NL3, DDHd, and SLy4 crusts, respectively. The impact of the crust is only of 2%. A similar dependency is seen for $\Lambda(M)$ but with a lower correlation value. We have, therefore, confirmed with our EoS sets the results presented in [68] concerning the relations $\Lambda \sim C^{-6}$ and $\Lambda \sim M^{-6}$, and shown that the impact of the crust is small. It was also shown that, for a fixed NS mass M_i , the relation $\Lambda \sim R^\beta$ depends on the crust and on the NS mass. The correlation becomes stronger as the NS mass increases, and it is almost exact and crust independent for massive NS: a correlation of 0.99 for both NL3 and SLy4 crusts and 0.97 for DDHd was obtained for $M \geq 1.8M_\odot$ with $\beta \sim 8 - 9$.

The effective tidal deformability $\tilde{\Lambda}$ is directly determined from the gravitational-wave signal of a neutron star merger, and, therefore it is important to identify possible correlations between this quantity and NS properties. We have found a perfect power relation between M_{chirp} and $\tilde{\Lambda}$. The dependence $M_{\text{chirp}} \propto \tilde{\Lambda}^\beta$ has $\beta = -5.824, -5.910,$ and -5.781 for, the NL3, DDHd, and SLy4 crusts, respectively. The crust impact is around 2%. We have also analyzed how Λ_{M_i} can be predicted from the effective binary tidal deformability $\tilde{\Lambda}$ for $M_{\text{chirp}} = 1.186M_\odot$, the value obtained for the GW170817 event. We first studied the $M_i = 1.4M_\odot$ case, showing

an almost perfect correlation and crust independence between $\Lambda_{1.4M_\odot}$ and $\tilde{\Lambda}$. The relation $\Lambda_{1.4M_\odot} = \beta\tilde{\Lambda} + \alpha$ shows an overall uncertainty below 5% for $q = 0.947$ and 10% for lower q values. This result is interesting because even if a $1.4M_\odot$ NS is not part of the binary, it is still possible to determine its tidal deformability, $\Lambda_{1.4M_\odot}$, with an accuracy of at least $\approx 10\%$.

In [74, 75], the authors have obtained a high correlation between $\tilde{\Lambda}$ and the radius of the M_1 star, R_1 . We have confirmed the validity of the empirical relation $\tilde{\Lambda} \propto R_1^\beta$ for $0.73 < M_1/M_2 < 1.0$, however, we could also verify that the crust shows an impact of about 14%. The values $\beta = 6.554, 5.729, \text{ and } 6.553$ have been determined for the NL3, DDHd, and SLy4 crusts, respectively.

We have explored the possibility of constraining the upper limits of both Λ_{M_i} and R_{M_i} from the LIGO/Virgo upper bound $\tilde{\Lambda} = 720$ [13]. For a $1.4M_\odot$ NS, the constraints obtained from $\Lambda_{1.4M_\odot}(q, \tilde{\Lambda} = 720)$ are in between 636 at $q = 0.74$ and 617 at $q = 0.99$ for the NL3 crust; similar values were found for the SLy4 crust and slightly smaller values for the DDHd crust. Imposing $\tilde{\Lambda} = 720$, we have obtained $12.70 < R_{1.4M_\odot}^{\text{upper}} < 12.78$ km as an upper bound for the NL3 and SLy4 crusts, while DDHd shows values $\approx 1\%$ larger. If, besides, we consider 300 as a lower bound on $\tilde{\Lambda}$ for the GW170817 event, as determined from the analysis of the electromagnetic counterpart in [63], a lower limit of $11.40 < R_{1.4M_\odot}^{\text{lower}} < 11.48$ km was established for the NL3 and SLy4 crusts, and $\approx 1\%$ larger for the DDHd crust.

We confirm the very strong correlation between $\tilde{\Lambda}$ and

M_{chirp} obtained in [68]. For our EoS sets, the dependence $\tilde{\Lambda} \sim M_{\text{chirp}}^\beta$ was obtained, with $-5.92 < \beta < -5.78$ very close to -6 . In [68], it was proposed that $\Lambda_1/\Lambda_2 = q^a$, with $a = 6$ since $R_1 \approx R_2$. Allowing the chirp mass to vary in a reasonable range taking into account the event GW170817, we have obtained $5.25 < a < 6.91$ which give rise to larger values of the ratio Λ_1/Λ_2 , up to 50% (15%) larger at the lower (upper) limit than when compared to the results obtained in [68]. Besides, we have shown that this correlation depends on the chirp mass M_{chirp} and that it can be described to a very good approximation as $\Lambda_1/\Lambda_2 = q^a$, with $a \sim \sqrt{M_{\text{chirp}}}$, for $1.0 \leq M_{\text{chirp}}/M_\odot \leq 1.3$.

Acknowledgments: This work was partly supported by Fundação para a Ciência e Tecnologia, Portugal, under the projects UID/FIS/04564/2016 and POCI-01-0145-FEDER-029912 with financial support from POCI, in its FEDER component, and by the FCT/MCTES budget through national funds (OE), and by PHAROS COST Action CA16214.

Appendix A: Predictions for $\Lambda_{M_i}(q, \tilde{\Lambda})$ and $R_{M_i}(q, \tilde{\Lambda})$

Herein, we show the predictions for $\Lambda_{M_i}(q, \tilde{\Lambda})$ and $R_{M_i}(q, \tilde{\Lambda})$, using the correlation analysis $\text{Corr}[\Lambda_{M_i}, \tilde{\Lambda}]$ and $\text{Corr}[R_{M_i}, \tilde{\Lambda}]$. Tables VI and VII contain the Λ_{M_i} and R_{M_i} bounds, respectively, using $\tilde{\Lambda} = 300$ and 720 as constraints.

-
- [1] Z. Arzoumanian *et al.* (NANOGrav), *Astrophys. J. Suppl.* **235**, 37 (2018), arXiv:1801.01837 [astro-ph.HE].
- [2] E. Fonseca *et al.*, *Astrophys. J.* **832**, 167 (2016), arXiv:1603.00545 [astro-ph.HE].
- [3] P. Demorest, T. Pennucci, S. Ransom, M. Roberts, and J. Hessels, *Nature* **467**, 1081 (2010).
- [4] J. Antoniadis, P. C. C. Freire, N. Wex, T. M. Tauris, R. S. Lynch, M. H. van Kerkwijk, M. Kramer, C. Bassa, V. S. Dhillon, T. Driebe, J. W. T. Hessels, V. M. Kaspi, V. I. Kondratiev, N. Langer, T. R. Marsh, M. A. McLaughlin, T. T. Pennucci, S. M. Ransom, I. H. Stairs, J. van Leeuwen, J. P. W. Verbiest, and D. G. Whelan, *Science* **340**, 448 (2013).
- [5] H. T. Cromartie *et al.*, (2019), 10.1038/s41550-019-0880-2, arXiv:1904.06759 [astro-ph.HE].
- [6] Z. Arzoumanian, K. C. Gendreau, C. L. Baker, T. Cazeau, P. Hestnes, J. W. Kellogg, S. J. Kenyon, R. P. Kozon, K. C. Liu, S. S. Manthripragada, C. B. Markwardt, A. L. Mitchell, J. W. Mitchell, C. A. Monroe, T. Okajima, S. E. Pollard, D. F. Powers, B. J. Savadkin, L. B. Winternitz, P. T. Chen, M. R. Wright, R. Foster, G. Prigozhin, R. Remillard, and J. Doty, “The neutron star interior composition explorer (NICER): mission definition,” in *Proceedings of the SPIE, Volume 9144, id. 914420 9 pp. (2014)*, Society of Photo-Optical Instrumentation Engineers (SPIE) Conference Series, Vol. 9144 (2014) p. 914420.
- [7] C. Motch, J. Wilms, D. Barret, W. Becker, S. Bogdanov, L. Boirin, S. Corbel, E. Cackett, S. Campana, D. de Martino, F. Haberl, J. in’t Zand, M. Méndez, R. Mignani, J. Miller, M. Orío, D. Psaltis, N. Rea, J. Rodriguez, A. Rozanska, A. Schwöpe, A. Steiner, N. Webb, L. Zampieri, and S. Zane, arXiv e-prints, arXiv:1306.2334 (2013), arXiv:1306.2334 [astro-ph.HE].
- [8] A. L. Watts, W. Yu, J. Poutanen, S. Zhang, S. Bhat-tacharyya, S. Bogdanov, L. Ji, A. Patruno, T. E. Riley, P. Bakala, A. Baykal, F. Bernardini, I. Bombaci, E. Brown, Y. Cavecchi, D. Chakrabarty, J. Chenevez, N. Degenaar, M. Del Santo, T. Di Salvo, V. Doroshenko, M. Falanga, R. D. Ferdman, M. Feroci, A. F. Gambino, M. Ge, S. K. Greif, S. Guillot, C. Gungor, D. H. Hartmann, K. Hebeler, A. Heger, J. Homan, R. Iaria, J. i. Zand, O. Kargaltsev, A. Kurkela, X. Lai, A. Li, X. Li, Z. Li, M. Linares, F. Lu, S. Mahmoodifar, M. Méndez, M. Coleman Miller, S. Morsink, J. Nättilä, A. Possenti, C. Prescod-Weinstein, J. Qu, A. Riggio, T. Salmi, A. Sanna, A. Santangelo, H. Schatz, A. Schwenk, L. Song, E. Šrámková, B. Stappers, H. Stiele, T. Strohmayer, I. Tews, L. Tolos, G. Török, D. Tsang, M. Urbanec, A. Vacchi, R. Xu, Y. Xu, S. Zane, G. Zhang, S. Zhang, W. Zhang, S. Zheng, and X. Zhou, *Science China Physics, Mechanics, and Astronomy* **62**, 29503 (2019),

Bound: $\tilde{\Lambda} = 720$							
Crust	q	$\Lambda_{1.1M_{\odot}}$	$\Lambda_{1.2M_{\odot}}$	$\Lambda_{1.3M_{\odot}}$	$\Lambda_{1.4M_{\odot}}$	$\Lambda_{1.5M_{\odot}}$	$\Lambda_{1.6M_{\odot}}$
NL3	0.74	2331 ± 4	1480 ± 2	962 ± 1	636 ± 0	427 ± 1	289 ± 1
NL3	0.99	2268 ± 4	1438 ± 2	934 ± 1	617 ± 0	413 ± 1	279 ± 1
SLy4	0.74	2321 ± 6	1477 ± 3	963 ± 1	639 ± 1	429 ± 1	291 ± 1
SLy4	0.99	2251 ± 6	1432 ± 3	932 ± 1	618 ± 0	414 ± 1	280 ± 1
DDHd	0.74	2396 ± 7	1500 ± 3	962 ± 1	628 ± 1	416 ± 1	278 ± 1
DDHd	0.99	2340 ± 7	1465 ± 3	940 ± 1	614 ± 1	407 ± 1	272 ± 1

Bound: $\tilde{\Lambda} = 300$							
Crust	q	$\Lambda_{1.1M_{\odot}}$	$\Lambda_{1.2M_{\odot}}$	$\Lambda_{1.3M_{\odot}}$	$\Lambda_{1.4M_{\odot}}$	$\Lambda_{1.5M_{\odot}}$	$\Lambda_{1.6M_{\odot}}$
NL3	0.74	1175 ± 6	691 ± 2	410 ± 1	244 ± 1	144 ± 1	83 ± 1
NL3	0.99	1192 ± 6	701 ± 2	415 ± 1	247 ± 1	146 ± 1	84 ± 1
SLy4	0.74	1143 ± 8	681 ± 3	410 ± 1	247 ± 1	149 ± 1	88 ± 2
SLy4	0.99	1156 ± 9	687 ± 4	412 ± 1	248 ± 1	149 ± 1	88 ± 1
DDHd	0.74	1187 ± 13	692 ± 5	409 ± 2	242 ± 2	142 ± 2	82 ± 2
DDHd	0.99	1228 ± 15	712 ± 6	419 ± 2	247 ± 1	145 ± 2	83 ± 2

Table VI. Predictions for $\Lambda_{M_i}(q, \tilde{\Lambda})$ for $q = 0.74$ and 0.99 using $\tilde{\Lambda} = 720$ and 300 . The uncertainties define the 95% confidence interval region.

Radius Upper Bound: $\tilde{\Lambda} = 720$							
Crust	q	$R_{1.1M_{\odot}}$	$R_{1.2M_{\odot}}$	$R_{1.3M_{\odot}}$	$R_{1.4M_{\odot}}$	$R_{1.5M_{\odot}}$	$R_{1.6M_{\odot}}$
NL3	0.74	12.53 ± 0.01	12.62 ± 0.01	12.70 ± 0.01	12.78 ± 0.00	12.84 ± 0.00	12.90 ± 0.00
NL3	0.99	12.47 ± 0.01	12.56 ± 0.01	12.64 ± 0.01	12.71 ± 0.00	12.77 ± 0.00	12.82 ± 0.00
SLy4	0.74	12.51 ± 0.01	12.61 ± 0.01	12.70 ± 0.01	12.78 ± 0.01	12.85 ± 0.01	12.90 ± 0.01
SLy4	0.99	12.44 ± 0.01	12.54 ± 0.01	12.62 ± 0.01	12.70 ± 0.01	12.76 ± 0.01	12.82 ± 0.01
DDHd	0.74	12.78 ± 0.02	12.83 ± 0.02	12.88 ± 0.01	12.91 ± 0.01	12.94 ± 0.01	12.96 ± 0.01
DDHd	0.99	12.72 ± 0.02	12.77 ± 0.02	12.81 ± 0.01	12.85 ± 0.01	12.88 ± 0.01	12.90 ± 0.01

Radius Lower Bound: $\tilde{\Lambda} = 300$							
Crust	q	$R_{1.1M_{\odot}}$	$R_{1.2M_{\odot}}$	$R_{1.3M_{\odot}}$	$R_{1.4M_{\odot}}$	$R_{1.5M_{\odot}}$	$R_{1.6M_{\odot}}$
NL3	0.74	11.53 ± 0.01	11.52 ± 0.01	11.50 ± 0.01	11.46 ± 0.01	11.40 ± 0.01	11.32 ± 0.01
NL3	0.99	11.55 ± 0.01	11.54 ± 0.01	11.52 ± 0.01	11.48 ± 0.01	11.42 ± 0.01	11.33 ± 0.01
SLy4	0.74	11.42 ± 0.02	11.43 ± 0.01	11.43 ± 0.01	11.40 ± 0.01	11.36 ± 0.01	11.29 ± 0.01
SLy4	0.99	11.44 ± 0.02	11.45 ± 0.01	11.44 ± 0.01	11.41 ± 0.01	11.37 ± 0.01	11.30 ± 0.01
DDHd	0.74	11.67 ± 0.03	11.64 ± 0.03	11.60 ± 0.02	11.54 ± 0.02	11.47 ± 0.02	11.38 ± 0.02
DDHd	0.99	11.74 ± 0.04	11.70 ± 0.03	11.65 ± 0.02	11.59 ± 0.02	11.51 ± 0.02	11.41 ± 0.02

Table VII. Predictions for $R_{M_i}(q, \tilde{\Lambda})$ (in km) for $q = 0.74$ and 0.99 using $\tilde{\Lambda} = 720$ and 300 . The uncertainties define the 95% confidence interval region.

- arXiv:1812.04021 [astro-ph.HE].
- [9] M. C. Miller, F. K. Lamb, A. J. Dittmann, S. Bogdanov, Z. Arzoumanian, K. C. Gendreau, S. Guillot, A. K. Harding, W. C. G. Ho, J. M. Lattimer, R. M. Ludlam, S. Mahmoodifar, S. M. Morsink, P. S. Ray, T. E. Strohmayer, K. S. Wood, T. Enoto, R. Foster, T. Oka-jima, G. Prigozhin, and Y. Soong, *The Astrophysical Journal* **887**, L24 (2019).
- [10] T. E. Riley, A. L. Watts, S. Bogdanov, P. S. Ray, R. M. Ludlam, S. Guillot, Z. Arzoumanian, C. L. Baker, A. V. Bilous, D. Chakrabarty, K. C. Gendreau, A. K. Harding, W. C. G. Ho, J. M. Lattimer, S. M. Morsink, and T. E. Strohmayer, *The Astrophysical Journal* **887**, L21 (2019).
- [11] A. Watts *et al.*, *Proceedings, Advancing Astrophysics with the Square Kilometre Array (AASKA14): Giardino Naxos, Italy, June 9-13, 2014*, PoS **AASKA14**, 043 (2015), arXiv:1501.00042 [astro-ph.SR].
- [12] B. P. Abbott *et al.* (LIGO Scientific, Virgo), *Phys. Rev. Lett.* **119**, 161101 (2017), arXiv:1710.05832 [gr-qc].
- [13] B. P. Abbott *et al.* (LIGO Scientific, Virgo), *Phys. Rev.* **X9**, 011001 (2019), arXiv:1805.11579 [gr-qc].
- [14] B. P. Abbott *et al.* (Virgo, LIGO Scientific), *Phys. Rev. Lett.* **121**, 161101 (2018), arXiv:1805.11581 [gr-qc].

- [15] B. P. Abbott *et al.* (LIGO Scientific, Virgo, Fermi-GBM, INTEGRAL), *Astrophys. J.* **848**, L13 (2017), arXiv:1710.05834 [astro-ph.HE].
- [16] B. P. Abbott *et al.* (LIGO Scientific, Virgo, Fermi-GBM, INTEGRAL, IceCube, AstroSat Cadmium Zinc Telluride Imager Team, IPN, Insight-Hxmt, ANTARES, Swift, AGILE Team, 1M2H Team, Dark Energy Camera GW-EM, DES, DLT40, GRAWITA, Fermi-LAT, ATCA, ASKAP, Las Cumbres Observatory Group, OzGrav, DWF (Deeper Wider Faster Program), AST3, CAAS-TRO, VINROUGE, MASTER, J-GEM, GROWTH, JAGWAR, CaltechNRAO, TTU-NRAO, NuSTAR, Pan-STARRS, MAXI Team, TZAC Consortium, KU, Nordic Optical Telescope, ePESSTO, GROND, Texas Tech University, SALT Group, TOROS, BOOTES, MWA, CALET, IKI-GW Follow-up, H.E.S.S., LOFAR, LWA, HAWC, Pierre Auger, ALMA, Euro VLBI Team, Pi of Sky, Chandra Team at McGill University, DFN, ATLAS Telescopes, High Time Resolution Universe Survey, RIMAS, RATIR, SKA South Africa/MeerKAT), *Astrophys. J.* **848**, L12 (2017), arXiv:1710.05833 [astro-ph.HE].
- [17] D. Radice, S. Bernuzzi, W. Del Pozzo, L. F. Roberts, and C. D. Ott, *Astrophys. J.* **842**, L10 (2017), arXiv:1612.06429 [astro-ph.HE].
- [18] D. Radice, A. Perego, F. Zappa, and S. Bernuzzi, *Astrophys. J.* **852**, L29 (2018), arXiv:1711.03647 [astro-ph.HE].
- [19] A. Bauswein, N.-U. Friedrich Bastian, D. Blaschke, K. Chatziioannou, J. A. Clark, T. Fischer, H.-T. Janka, O. Just, M. Oertel, and N. Stergioulas, *AIP Conf. Proc.* **2127**, 020013 (2019), arXiv:1904.01306 [astro-ph.HE].
- [20] M. W. Coughlin *et al.*, *Mon. Not. Roy. Astron. Soc.* **480**, 3871 (2018), arXiv:1805.09371 [astro-ph.HE].
- [21] Y.-Z. Wang, D.-S. Shao, J.-L. Jiang, S.-P. Tang, X.-X. Ren, F.-W. Zhang, Z.-P. Jin, Y.-Z. Fan, and D.-M. Wei, *Astrophys. J.* **877**, 2 (2019), arXiv:1811.02558 [astro-ph.HE].
- [22] J. Margueron, R. Hoffmann Casali, and F. Gulminelli, *Phys. Rev.* **C97**, 025805 (2018), arXiv:1708.06894 [nucl-th].
- [23] J. Margueron, R. Hoffmann Casali, and F. Gulminelli, *Phys. Rev.* **C97**, 025806 (2018), arXiv:1708.06895 [nucl-th].
- [24] N.-B. Zhang, B.-A. Li, and J. Xu, *Astrophys. J.* **859**, 90 (2018), arXiv:1801.06855 [nucl-th].
- [25] J. Margueron and F. Gulminelli, *Phys. Rev.* **C99**, 025806 (2019), arXiv:1807.01729 [nucl-th].
- [26] I. Bombaci and U. Lombardo, *Phys. Rev. C* **44**, 1892 (1991).
- [27] J. S. Read, B. D. Lackey, B. J. Owen, and J. L. Friedman, *Phys. Rev. D* **79**, 124032 (2009).
- [28] F. Özel and D. Psaltis, *Phys. Rev. D* **80**, 103003 (2009).
- [29] A. W. Steiner, J. M. Lattimer, and E. F. Brown, *Astrophys. J.* **722**, 33 (2010), arXiv:1005.0811 [astro-ph.HE].
- [30] C. A. Raithel, F. Özel, and D. Psaltis, *Astrophys. J.* **831**, 44 (2016), arXiv:1605.03591 [astro-ph.HE].
- [31] L. Lindblom, *Phys. Rev.* **D82**, 103011 (2010), arXiv:1009.0738 [astro-ph.HE].
- [32] I. Tews, J. Margueron, and S. Reddy, *Phys. Rev.* **C98**, 045804 (2018), arXiv:1804.02783 [nucl-th].
- [33] E. Annala, T. Gorda, A. Kurkela, J. Nättilä, and A. Vuorinen, (2019), arXiv:1903.09121 [astro-ph.HE].
- [34] J. S. Read, B. D. Lackey, B. J. Owen, and J. L. Friedman, *Phys. Rev.* **D79**, 124032 (2009), arXiv:0812.2163 [astro-ph].
- [35] Z. Carson, A. W. Steiner, and K. Yagi, *Phys. Rev.* **D99**, 043010 (2019), arXiv:1812.08910 [gr-qc].
- [36] Z. Carson, A. W. Steiner, and K. Yagi, *Phys. Rev.* **D100**, 023012 (2019), arXiv:1906.05978 [gr-qc].
- [37] M. Fortin, C. Providencia, A. R. Raduta, F. Gulminelli, J. L. Zdunik, P. Haensel, and M. Bejger, *Phys. Rev.* **C94**, 035804 (2016), arXiv:1604.01944 [astro-ph.SR].
- [38] M. Ferreira, M. Fortin, T. Malik, B. Agrawal, and C. Providência, *Phys. Rev. D* **101**, 043021 (2020), arXiv:1912.11131 [nucl-th].
- [39] D. H. Youngblood, H. L. Clark, and Y. W. Lui, *Phys. Rev. Lett.* **82**, 691 (1999).
- [40] J. Margueron and E. Khan, *Phys. Rev.* **C86**, 065801 (2012), arXiv:1203.2134 [nucl-th].
- [41] B.-A. Li and X. Han, *Phys. Lett.* **B727**, 276 (2013), arXiv:1304.3368 [nucl-th].
- [42] J. M. Lattimer and Y. Lim, *Astrophys. J.* **771**, 51 (2013).
- [43] J. R. Stone, N. J. Stone, and S. A. Moszkowski, *Phys. Rev.* **C89**, 044316 (2014), arXiv:1404.0744 [nucl-th].
- [44] M. Oertel, M. Hempel, T. Klähn, and S. Typel, *Rev. Mod. Phys.* **89**, 015007 (2017).
- [45] M. Farine, J. M. Pearson, and F. Tondeur, *Nucl. Phys.* **A615**, 135 (1997).
- [46] J. N. De, S. K. Samaddar, and B. K. Agrawal, *Phys. Rev.* **C92**, 014304 (2015), arXiv:1506.06461 [nucl-th].
- [47] C. Mondal, B. K. Agrawal, J. N. De, and S. K. Samaddar, *Phys. Rev.* **C93**, 044328 (2016).
- [48] T. Malik, N. Alam, M. Fortin, C. Providência, B. K. Agrawal, T. K. Jha, B. Kumar, and S. K. Patra, *Phys. Rev.* **C98**, 035804 (2018), arXiv:1805.11963 [nucl-th].
- [49] B.-A. Li, P. G. Krastev, D.-H. Wen, W.-J. Xie, and N.-B. Zhang, *AIP Conf. Proc.* **2127**, 020018 (2019).
- [50] F. Douchin and P. Haensel, *Astron. Astrophys.* **380**, 151 (2001), arXiv:astro-ph/0111092 [astro-ph].
- [51] S. S. Avancini, D. P. Menezes, M. D. Alloy, J. R. Marinelli, M. M. W. Moraes, and C. Providência, *Phys. Rev. C* **78**, 015802 (2008).
- [52] F. Grill, C. Providencia, and S. S. Avancini, *Phys. Rev.* **C85**, 055808 (2012), arXiv:1203.4166 [nucl-th].
- [53] F. Grill, H. Pais, C. Providência, I. Vidaña, and S. S. Avancini, *Phys. Rev.* **C90**, 045803 (2014), arXiv:1404.2753 [nucl-th].
- [54] G. A. Lalazissis, J. König, and P. Ring, *Phys. Rev.* **C55**, 540 (1997), arXiv:nucl-th/9607039 [nucl-th].
- [55] T. Gaitanos, M. Di Toro, S. Typel, V. Baran, C. Fuchs, V. Greco, and H. H. Wolter, *Nucl. Phys.* **A732**, 24 (2004).
- [56] H. Pais and C. Providência, *Phys. Rev.* **C94**, 015808 (2016), arXiv:1607.05899 [nucl-th].
- [57] A. Raduta and F. Gulminelli, *Phys. Rev. C* **82**, 065801 (2010), arXiv:1009.2226 [nucl-th].
- [58] H. Pais, W. G. Newton, and J. R. Stone, *Phys. Rev. C* **90**, 065802 (2014), arXiv:1411.1885 [nucl-th].
- [59] C. Ducoin, J. Margueron, C. Providencia, and I. Vidana, *Phys. Rev.* **C83**, 045810 (2011), arXiv:1102.1283 [nucl-th].
- [60] R. C. Tolman, *Phys. Rev.* **55**, 364 (1939).
- [61] J. R. Oppenheimer and G. M. Volkoff, *Phys. Rev.* **55**, 374 (1939).
- [62] T. Hinderer, *Astrophys. J.* **677**, 1216 (2008), arXiv:0711.2420 [astro-ph].

- [63] D. Radice and L. Dai, *The European Physical Journal A* **55** (2019), 10.1140/epja/i2019-12716-4.
- [64] A. Maselli, V. Cardoso, V. Ferrari, L. Gualtieri, and P. Pani, *Phys. Rev.* **D88**, 023007 (2013), arXiv:1304.2052 [gr-qc].
- [65] K. Yagi and N. Yunes, *Phys. Rept.* **681**, 1 (2017), arXiv:1608.02582 [gr-qc].
- [66] K. Yagi and N. Yunes, *Science* **341**, 365 (2013), arXiv:1302.4499 [gr-qc].
- [67] T. K. Chan, A. P. O. Chan, and P. T. Leung, *Phys. Rev. D* **93**, 024033 (2016).
- [68] S. De, D. Finstad, J. M. Lattimer, D. A. Brown, E. Berger, and C. M. Biwer, *Phys. Rev. Lett.* **121**, 091102 (2018), [Erratum: *Phys. Rev. Lett.*121,no.25,259902(2018)], arXiv:1804.08583 [astro-ph.HE].
- [69] G. Baym, C. Pethick, and P. Sutherland, *Astrophys. J.* **170**, 299 (1971).
- [70] J. W. Negele and D. Vautherin, *Nuclear Physics A* **207**, 298 (1973).
- [71] E. Annala, T. Gorda, A. Kurkela, and A. Vuorinen, *Phys. Rev. Lett.* **120**, 172703 (2018).
- [72] T. Malik, N. Alam, M. Fortin, C. Providência, B. K. Agrawal, T. K. Jha, B. Kumar, and S. K. Patra, *Phys. Rev.* **C98**, 035804 (2018), arXiv:1805.11963 [nucl-th].
- [73] F. J. Fattoyev, J. Piekarewicz, and C. J. Horowitz, *Phys. Rev. Lett.* **120**, 172702 (2018), arXiv:1711.06615 [nucl-th].
- [74] C. Raithel, F. Özel, and D. Psaltis, *Astrophys. J.* **857**, L23 (2018), arXiv:1803.07687 [astro-ph.HE].
- [75] C. A. Raithel, *Eur. Phys. J.* **A55**, 80 (2019), arXiv:1904.10002 [astro-ph.HE].
- [76] E. R. Most, L. R. Weih, L. Rezzolla, and J. Schaffner-Bielich, *Phys. Rev. Lett.* **120**, 261103 (2018).